18th Brazilian Congress of Thermal Sciences and Engineering
November 16-20, 2020 (Online)

ENC-2020-0615
NUMERICAL SIMULATION OF TURBULENT FLOW OVER AHMED BODY

Jalusa Maria da Silva Ferrari
GMEC, Universidade de Brasília, Brasília, Brazil
jalusaferrari@gmail.com

Fábio Matos Kayser
GMEC, Universidade de Brasília, Brasília, Brazil
fabio_mk_66@hotmail.com

Luciano Gonçalves Noleto
Universidade de Brasília, Brasília, Brazil
lucianonoleto@gmail.com

Jhon Nero Vaz Goulart
GMEC, Universidade de Brasília, Brasília, Brazil
jvazgoulart@gmail.com

Abstract. *The objective of the present paper is to evaluate the turbulent flow around the Ahmed body immersed in air to determine aerodynamic coefficients for different slant angles. The bidimensional non-stationary analysis of an incompressible flow around the Ahmed body is carried for three different rear angles which are 0°, 10° and 25°. The numerical simulations were performed under the same Reynolds number, Re = 94 000, based on the free streamwise velocity, u_∞, the longitudinal length of the Ahmed body, l, and the kinematic viscosity of the work fluid, ν. The additional diffusivity caused by the turbulent motion was approached using the Boussinesq's idea through the k-ω SST. In the paper, aerodynamic coefficients of drag and lift, pressure and velocity fields are presented to characterize the Ahmed body for different slant angles, as well as the flow detachment point, determined through the dimensionless skin friction factor distribution on the body's surface. Numerical simulations were compared with available results in open literature and showed agreement with other authors. The drag coefficient in the body with slant angle of 25° was found to matche with the drag coefficient equation proposed by Bello-Millán et al. (2016) as a function of Reynolds number.*

Keywords:*Ahmed body, Turbulent flow, Vehicular aerodynamics, Fluid mechanics, CFD.*

1. INTRODUCTION

Aerodynamics is the study of resulting forces from the movement of a fluid through a body and is an important part of the vehicle design process. The fuel consumption of a vehicle associated with its movement is directly related to aerodynamic characteristics, such as the aerodynamic drag of the vehicle which is expressed as the drag coefficient, Cd (Ortega and Salari, 2005).

The understanding of vehicular aerodynamics is accomplished by understanding the effect of the forces acting on the vehicle and how they arise. Consequently, detailed knowledge about flow characteristics and their relationship with body geometry is necessary for the design of new vehicles (Tunay et al., 2014). Ground vehicles are considered as blunt bodies near a flat surface that represents the ground. Complex structures, such as cavities and wheels under rotation, make the flow completely three-dimensional (Hucho, 2013). The drag vehicle is strongly depending on how the flow behaves along the vehicle.

The number of structures that are immersed in the fluid and, therefore, subjected to the forces acting on their surfaces is infinite. Each one is characterized by shape, size, sharp or round angles, which yields new forces distribution and, therefore, different drag and lift coefficients. For this reason, many bodies are studied using an approach that relates the flow characteristics with the one found around a flat plate, a sphere or a cylinder (Daugherty, 1989). The approach using a similar geometry is often used for a simplified study or as an initial design idea. The Ahmed body is a geometric simplification of an automobile vehicle and was chosen as the object of this study.

The Ahmed body was first presented in the study by Ahmed et al. (1984) with an experimental analysis of 3D flow in the body. The author' main objective was to verify the behavior of the drag coefficient, Cd, and the characteristics of

the flow according to the variation of the rear angle. Ahmed body combines the essential geometric characteristics that determine the shape, length and flow separation zone. For the numerical simulation, to describe the flow around Ahmed body is still a challenge. This occurs, mainly, due to the correct prediction of drag and lift coefficients consistent with the experiment carried out by Ahmed et al. (1984) and other authors on the subject.

The work aims to evaluate the aerodynamic drag and lift coefficient of Ahmed's body under a turbulent flow with Reynolds of 94000. It is also a purpose to identify the pressure distribution at the surface and the flow detachment point.

The main challenge that the work proposes is to simulate a problem notably tridimensional with a bidimensional geometry. The turbulence model used is k-ω SST. Furthermore, the work is also aimed to assess the relationship between the aerodynamics coefficients and slant angles, as well as the flow separation point.

2. GEOMETRY AND NUMERICAL PROCEDURE

2.1 Ahmed's body geometry

The dimensions of Ahmed body used in simulations of the present work are similar to that proposed by Ahmed et al. (1984) and are shown in Figure 1.

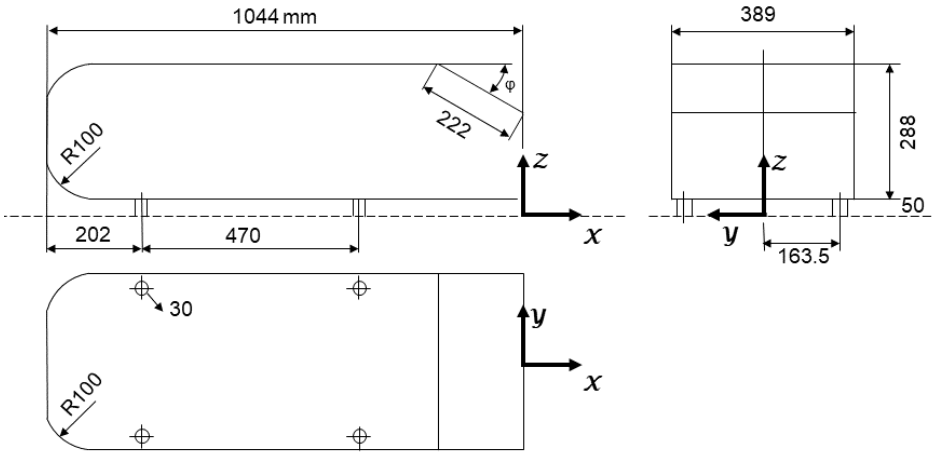

Figure 1. Dihedral view with dimensions used in the study of Ahmed body in Ahmed et al. (1984).

Figure 2 shows the computational domain with dimensions in terms of the longitudinal length, l, of the body. The body is 50 mm above ground in all simulations, assigned by the letter "h". The body domain is placed at 3.5 l, downstream the entrance and its rear part is 8l away from the domain's outlet. The upper free surface of the computational domain is far enough from the body, being 5 l. The free stream velocity $u_\infty = 1.29\ m/s$ is imposed at inlet (A). Velocity components in the other directions are zero ($v = w = 0$). The turbulent intensity at (A) is 1% applied at the free stream velocity. On body surfaces (B) non-slip conditions are applied. At the outlet (C) a null differential pressure condition is applied.

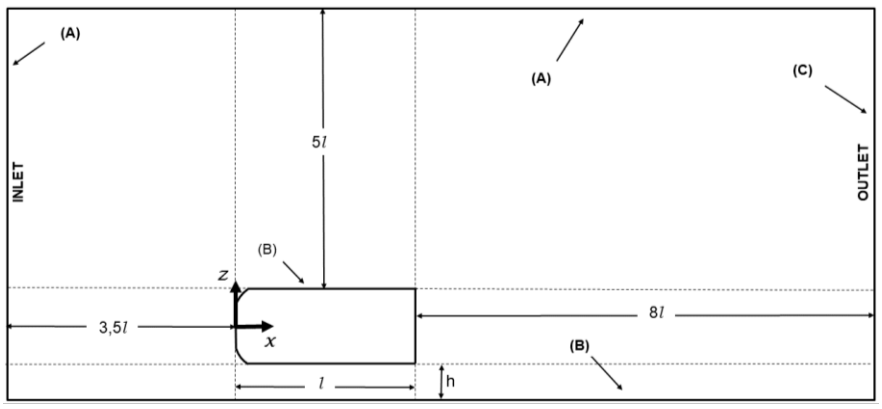

Figure 2. Description of the dimensionless computational domain based at Korkischko and Meneghini (2006).

The rear slat angles used are φ = 0°, 10° and 25°. The slant dimension was kept at 222 mm, as seen in Figure 3. Those angles were chosen to assess the relationship between the rear angle and the aerodynamic coefficients.

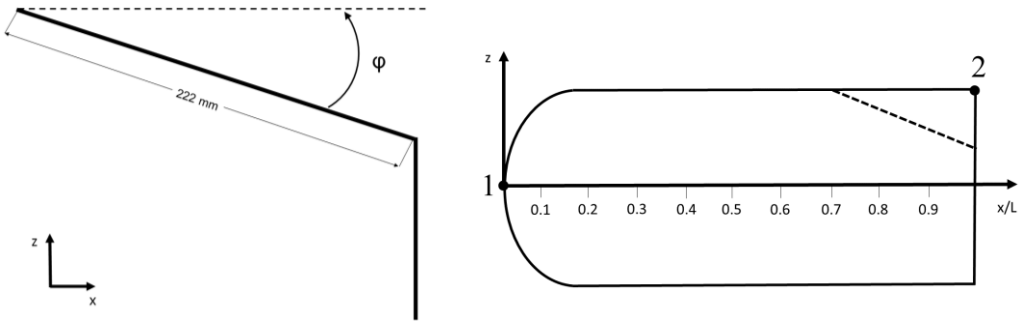

a) b)

Figure 3. Schematic of Ahmed body: a) Slant angle and b) Surface reference points.

A mesh analysis was performed in the stationary phase for the two-dimensional domain. The mesh was constructed with hexahedral volumes. The number of layers close to the wall was sufficient to obtain a y+ = 1 with a growth rate of 1.2 in relation to the node closest to the wall. The body with φ = 25° was used as a benchmark, since Bello-Millán et al. (2016) proposed an algebraic equation for drag evaluation over a vast Reynolds number range. The algebraic equation was tested face own their experimental values and other external authors, presenting a good agreement. According to Bello-Millán et al. (2016), the Eq. (1) is enough to provide Cd value for a Ahmed body for a Reynolds number ranging from 10^5 up to 6.96×10^6.

$$C_d = 0.3849 + 0.0603e^{-\frac{A}{0.5217}}$$
$$A = \frac{\mathrm{Re}_l}{10^6} \tag{1}$$

In the time-dependent simulation, the time step was $\Delta t = 1.1 \times 10^{-4}$ s and this was kept for the three simulated cases. Time discretization was carried out by using the the backward Euler scheme for time discretization. The advective terms of Navier-Stokes equations were solved by using Upwind Second Order scheme and the convergence criteria was set 10^{-5}, at least, for any equation.

To initialize the time-dependent runs stationary field was prescribed as a first time step response. Courant number was kept less than one. The averaging process for each quantity was carried out over for about 19 s, leading to 3 flow-through times.

2.2 Governing Equations

For incompressible flow, the mass conservation and the momentum are ruled, respectively, by Eq. (1) and (2):

$$\frac{\partial \overline{u_i}}{\partial x_i} = 0 \tag{2}$$

$$\frac{\partial \overline{u_i}}{\partial t} + \overline{u_j}\frac{\partial \overline{u_i}}{\partial x_j} = -\frac{1}{\rho}\frac{\partial \overline{P}}{\partial x_i} + \frac{\partial}{\partial x_j}\left[\left(\nu + \nu_t\right)\left(\frac{\partial \overline{u_i}}{\partial x_j} + \frac{\partial \overline{u_j}}{\partial x_i}\right)\right] \tag{3}$$

In Equations (2) and (3), $\overline{u_i}$ represents the velocity vector components, x_i is the spatial coordinates, $\overline{P}$ is the thermodynamic pressure, ρ is the fluid density, ν and ν_t are the molecular and turbulent kinematic viscosity, respectively. The additional momentum diffusivity, which is caused by the closure problem of the turbulence, is represented by the turbulent viscosity, ν_t, that is approximate through the Boussinesq's idea described as:

$$\tau_{ij} = \nu_t\left(\frac{\partial \overline{u_i}}{\partial x_j} + \frac{\partial \overline{u_j}}{\partial x_i}\right) - \frac{2}{3}\delta_{ij}k \tag{4}$$

τ_{ij} is the Reynolds tensor, which is obtained through the decomposition of the non-linear terms of Navier-Stokes equation, and *k* represents the turbulent kinetic energy. So, additional equations are needed to raise up the turbulent kinematic viscosity, which is computed as a function of the turbulent kinetic energy field, k, and the specific rate of dissipation, ω. The k-ω SST model is a two equations turbulence model first introduced by Menter (1994). The model combines the advantages from *k*-ε model and *k*-ω model by a blending function that switches whenever it is possible. According to Menter (1994), this two-equation model is ruled by the set of Equations in (5).

$$\begin{aligned}
&\frac{\partial k}{\partial t}+\overline{u}_j\frac{\partial k}{\partial x_j}=\frac{\tau_{ij}}{\rho}\frac{\partial \overline{u}_i}{\partial x_j}-\beta^*\omega k+\frac{\partial}{\partial x_j}\left[\left(\nu+\sigma_k\nu_t\right)\frac{\partial k}{\partial x_j}\right]\\
&\frac{\partial \omega}{\partial t}+\overline{u}_j\frac{\partial \omega}{\partial x_j}=\frac{\gamma\tau_{ij}}{\nu_t\rho}\frac{\partial \overline{u}_i}{\partial x_j}-\beta\omega^2+\frac{\partial}{\partial x_j}\left[\left(\nu+\sigma_\omega\nu_t\right)\frac{\partial \omega}{\partial x_j}\right]+2\left(1-F_1\right)\frac{\sigma_{\omega 2}}{\omega}\frac{\partial k}{\partial x_j}\frac{\partial \omega}{\partial x_j}
\end{aligned} \tag{5}$$

The blending function is F_1, which computes how far from the walls the problem is being solved and is defined as:

$$\begin{aligned}
&F_1=\tanh\left(\arg^4\right)\\
&\arg=\min\left[\max\left(\frac{\sqrt{k}}{\beta^*\omega d},\frac{500\nu}{d^2\omega}\right),\frac{4\rho\sigma_{\omega 2}k}{CD_{k\omega}d^2}\right]
\end{aligned} \tag{6}$$

$$\frac{a_1 k}{\max(a_1\omega,\Omega F_2)}$$

Finally, the turbulent kinematic viscosity is calculated through:

$$\nu_t=\frac{a_1 k}{\max(a_1\omega,\Omega F_2)} \tag{7}$$

Where Ω is the absolute value of the vorticity and a_1 is a closure coefficient that is set to 0.30.

3. RESULTS

3.1 Pressure and Friction Coefficients

In the next figures, the pressure and skin friction coefficients distribution on the body's surface are stressed. Both are shown in dimensionless form as follow:

$$\begin{aligned}
&Cp=\frac{p-p_0}{\frac{1}{2}\rho u_\infty^2}\\
&Cf=\frac{\tau_w}{\frac{\rho u_\infty^2}{2}}\sqrt{\mathrm{Re}}
\end{aligned} \tag{8}$$

Cp and Cf are the pressure and skin friction coefficients, respectively, ρ and τ_w are the pressure and the stress on the walls as a function of the position. Whereas P_o is the reference pressure, ρ is the fluid density and u_∞ is the free stream velocity in x-direction. The points shown in Fig. 2b marks reference points on the surface of Ahmed body. The following results are presented along the body between points 1 and 2.

The flow separation is characterized by an adverse pressure gradient, where fluid particles lose kinetic energy due to friction and also because of this gradient. This situation leads to a zero velocity at the surface and, consequently, a zero-stress location is highlighted, being straightforward to identify the flow detachment.

So, the flow separation takes place wherever τ_w is null on the contour of the body. The shear stress is null whenever:

$$\left.\frac{\partial \overline{u}}{\partial n}\right|=0 \text{ in } \Gamma \tag{9}$$

Figure 4 (a-c) shows the pressure coefficient at the upper side of the bodies for slant angles of 0°, 10° and 25°, respectively. It was observed that the presence of a slant changes the pressure coefficient distribution. For the three

cases, the maximum pressure was seen to take place at the frontal region, at the body's stagnation point, decreasing downstream.

For body with slant angle $\varphi = 0°$ the pressure coefficient assumes the minimal value at about x/L = 0.10, yielding Cp = -2.4. The same minimum value was observed for the two other cases, at x/L = 0.38 for the case with $\varphi = 10°$ and at x/L = 0.4 for $\varphi = 25°$. The simulations showed a remarkable difference with the presence of a rear slant angles, but it was not significant when the angle increased. However, it was interesting to note that highest pressure point, for the rear slant body of 25°, takes place at further position in comparison to the other geometries, meaning that the stagnation point has displaced towards the upper surface of the body.

In three cases, most part of the body presented negative values. Negative pressure values were well reported by Bruneau et al. (2014), who also stated that such low-pressure region behind the Ahmed body was resulted from the generated vortices at rear region. Although the behavior of the cp is different along the body, the same value was found at the end of them for any rear slant angle.

At around x/L = 0.7, the slant region begins for cases with $\varphi = 10^o$ and 25^o. It is possible to identify a local minimum, so that one can speculate to have a separation bubble or a flow jump happening in that region, as mentioned by Shadmani et al. (2018). Shadmani et al. (2018) also observed the Cp growth at slanted surface.

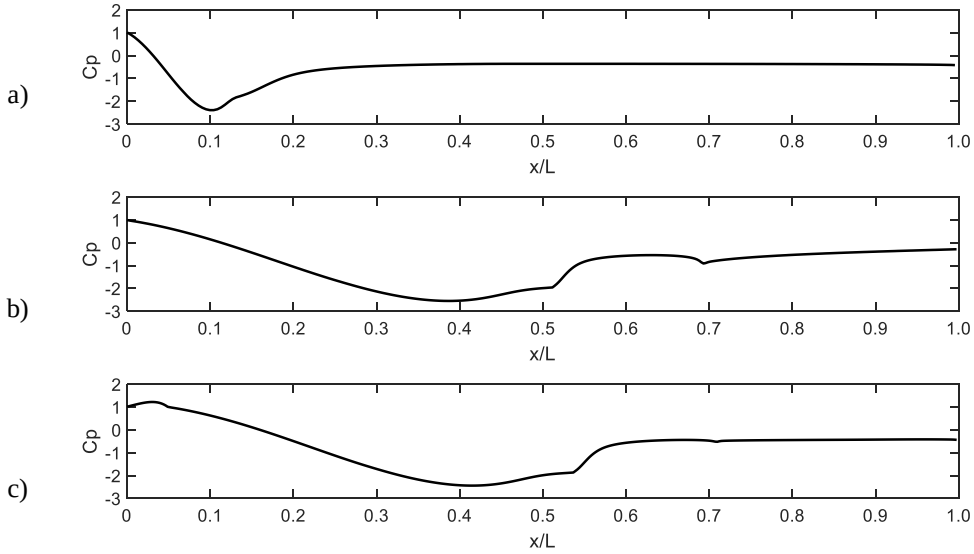

Figure 4 – Pressure coefficients for slant angles: a) 0º, b) 10º and c) 25º.

As said before the flow detachment can be identified through the skin friction coefficient, whenever Cf = 0. Figure 5 (a – c) shows the skin friction coefficient at the upper side of the bodies for the simulated slant angles of 0°, 10° and 25°. We can see the rear slat angle play important role on this regard. In the first case, $\varphi = 0°$, the flow is seen detached in the front region at about x/L = 0.12 and reattached at 0.19 (Fig. 5a). The skin friction coefficient decreases again near the body rear where it is expected a flow complete detachment behind the body.

With regard to the other two geometries, where the slant angle was increased, the skin friction coefficient distribution is completely different from the first case. In both pictures Fig. 5 (b and c), the null skin friction is seen at x/L = 0.49. The flow seems to reattaches again short after, indicating a separation bubble on the upper side of the body in both cases are the same. In Figure 5c, the reader can see the null skin friction again at x/L = 0.7, right where the slanted region begins. It is interesting to note that the slat increasing from 10° to 25° yields a different Cf distribution nearby the rear part of the body. The $\varphi = 10°$ body simulation did not show null Cf point after the reattaching flow.

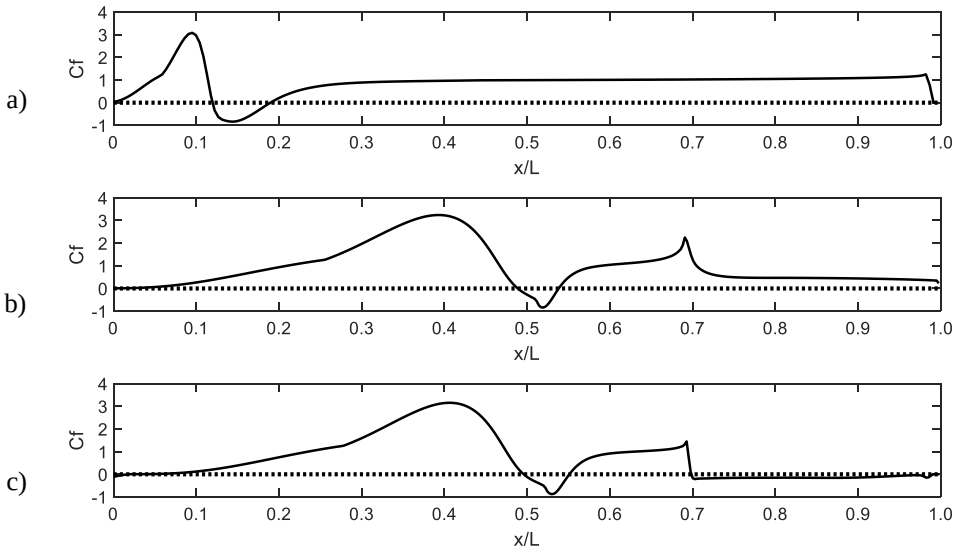

Figure 5 – Skin friction coefficients for slant angles: a) 0º, b) 10º and c) 25º.

3.2 Q Criterion

To identify coherent structures around the body, it was used the *Q* criterion, first proposed by Hunt et al. (1988). The idea behind the analyses is to discover the flow regions where the vorticity overpasses the shear strain rate. The *Q* parameter is then defined here as:

$$Q = \frac{1}{2}\left(|\omega|^2 - |S|^2\right) \tag{10}$$

where **S** is the shear strain rate tensor and **ω** is the rotation rate tensor and are defined as:

$$S_{ij} = \frac{1}{2}\left(\frac{\partial U_i}{\partial x_j} + \frac{\partial U_j}{\partial x_i}\right) \tag{11}$$

$$\omega = \nabla \times \vec{u}$$

Positive *Q* values indicates regions where the vorticity overcomes shear strain rate. A criterion to identify the presence of a vortical coherent structure is to inquire a surface where *Q* assumes positive values, called threshold. Figure 6 shows the structures observed through the *Q* criterion around the body.

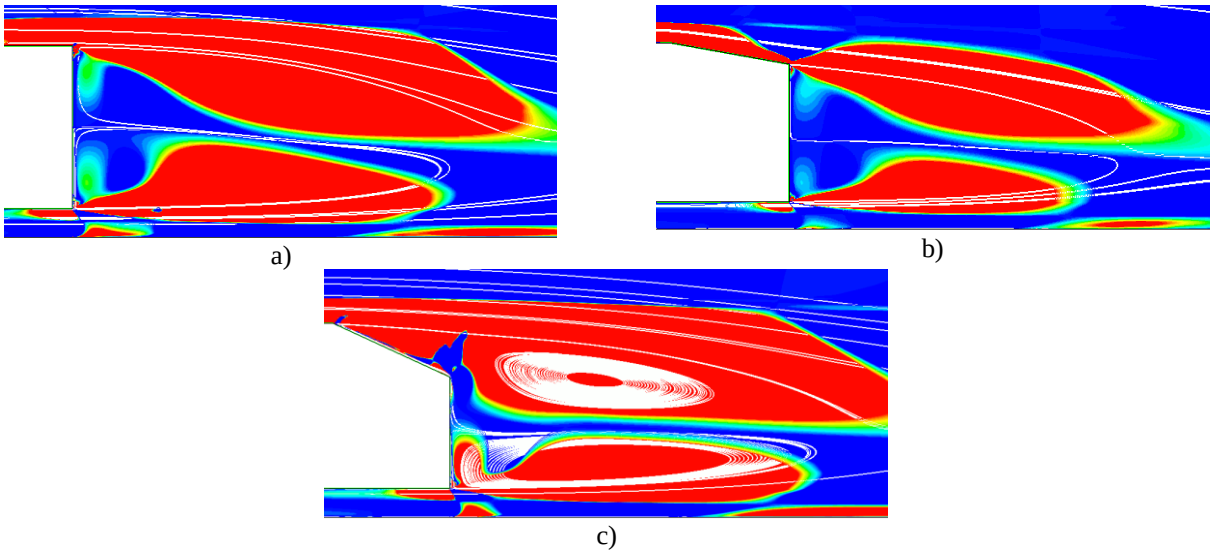

Figure 6 – Streamlines and coherent structures evaluated by *Q* criterion: a) 0º, b) 10º and c) 25º.

According to Möller and Silvestrini (2004), a series of coherent structures are generated in flows through blunt bodies and is possible to identify two as fundamentals with static asymmetry. Coherent structures can be defined as a large-scale turbulent fluid mass with correlated and phase vorticity in the fluid. Both appear in low Reynolds numbers as a characteristic of the flow symmetry break, but are still observed in high Reynolds values typical of ground vehicles.

As seen by Minguez and Pasquetti (2008) and Zhang et al. (2015), two larges counter-rotating trailing vortices were formed behind the body. In fact, in Fig 6a, the instantaneous streamlines suggest two recirculation bubbles, that show little differences in size. Such difference becomes even more evident as the slant angle is increased.

Also, Cf indicated that in the body with slant of 10º the flow detaches only after the slanted region ends. The streamlines in Fig. 6b show this behavior and allow the reader to visualize the difference when compared with the body of 25º in Fig. 6c, where the flow detaches as soon as the slant begins.

3.3 Drag Coefficients

In the present work, the Reynolds number is lower than that used in the Ahmed et al. (1984) in their experiments. Thus, higher values for the drag coefficient are expected than those obtained by Ahmed et al. (1984). This behavior was observed by Thacker et al. (2012), Dobrev and Massouh (2014) and Bello-Millán et al. (2016). Figure 7a shows the values of drag coefficients obtained in the simulations.

First of all, our test case (body with φ= 25°) reached a really good agreement with the Eq. 1, proposed by Bello-Millán et al. (2016) and with the work of Rafee and Moghimi (2018) for the same Reynolds number. According to Eq. 1 the Cd should be found at 0.44. In our computation we found Cd = 0.48.

When the other two bodies were analyzed different behavior were found. The lowest drag coefficient was found in the body of φ = 10° and the higher one in the body with whose rear slat angle is φ = 0°. After decreasing from 0° to 10° degrees the Cp almost recovers its value again reaching Cd about 0.48.

The growth behavior observed for these three slant angles were seen by Ahmed et al. (1984). The authors found that a slant angle of 0º leads to a high drag coefficient, but there is also a range of angles that induce more drag on the body. The drag coefficient decreases as the angle is increased from 0º and increases again until it reaches its critical angle, where the coefficient is maximum. After the critical angles, the drag coefficient falls again. For Re = 4.29×10^6, this critical angle was 30º. In the regime studied in the present work, this critical angle could be around 25º.

Figure 7b shows the relationship between the drag portion due to pressure drag Cd_p and the total drag coefficient of the body Cd. The Cd_p/Cd ratio was found to be from 0.95 up to 0.70, indication that the slant rear angle becomes the body less blunt. See that the null rear slant yields a Cd_p/Cd ratio more than 95%, very typical value found in circular cylinders and blunt bodies.

It is noteworthy the fact that the drag pressure decreases as the slant angle increases, which is very well justified since the area behind the body decreases as the slant rear angle becomes sharper.

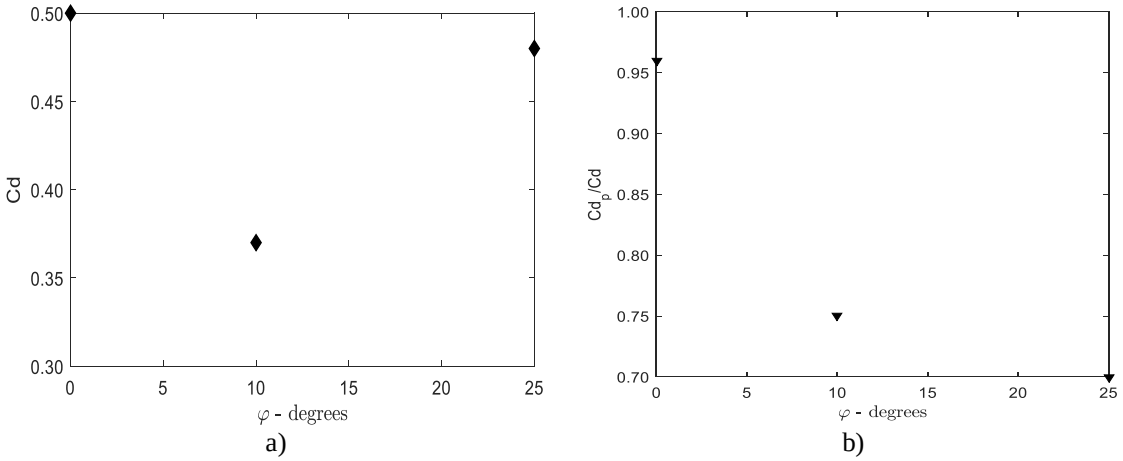

Figure 7 – a) Drag coefficient and b) Percentage of pressure drag on Ahmed body for Re = 94000.

4. CONCLUSIONS

In the present work, the turbulent flow around Ahmed body was evaluated through time-dependent simulations of the two-dimensional body. The simulations were made for Reynolds number 94 000 for three different rear slant angles, ranging from 0° up to 25 °. The turbulence model adopted was the k-ω SST.

It was seen that the pressure coefficient distribution was disturbed by the slant presence. In fact, the stagnation point has been displaced towards the upper surface of the body as slant was increased. In all three cases, Cp tends to present negative values along the body's length as seen by Bruneau et al. (2014).

The skin friction coefficient was equally affected by the slant presence. For $\varphi = 0^o$, there was an evidence of flow detachment at the upper side of the body, nearby x/L = 0.1. However, there was no evidence of detachment at the end of the body. On the other hand, for the following simulated cases, the skin friction showed points of detachment and reattachment along the body, at almost same position x/L = 0.49. Near the body rear, where it is expected that the flow detaches, Cf decreased. For $\varphi = 25^o$, Cf showed a detachment starting point at the slanted surface. The recirculation bubble over the body was displaced in comparison with the case $\varphi = 0^o$ and the other two cases.

The drag coefficient for $\varphi = 25°$ was found accordingly the equation proposed by Bello-Millán et al. (2016) and agrees with the studies of Rafee and Moghimi (2018). The furthered findings, $\varphi = 0°$ and 10°, showed the Cp recover for $\varphi > 10°$. Further, as the rear slant angle increases the body was seen less blunt, the Cd_p/Cd – ratio was seen decreasing as the rear angle increases.

5. ACKNOWLEDGEMENTS

The first author thanks to FAPDF for supporting her with financial resources through the projects n° 193.001.158/2015, 193.001356/2016.

The second author would like to thank the Coordenação de Aperfeiçoamento de Pessoal de Nível Superior - Brasil (CAPES) - Finance Code 001, for supporting him during this research with a fellowship.

Prof. Jhon Goulart is also thankful to CnPQ and FAPDF for supporting him with financial resources through the projects n° 193.001.158/2015, 193.001356/2016 and 408869/2016-0.

6. REFERENCES

Ahmed, S. R.; Ramm, G.; Faltin, G. "Some salient features of the time-averaged ground vehicle wake". *SAE Transactions*, JSTOR, p. 473–503, 1984.

Bello-Millán, F. et al. "Experimental study on Ahmed's body drag coefficient for different yaw angles". *Journal of Wind Engineering and Industrial Aerodynamics*, Elsevier, v. 157, p. 140–144, 2016.

Bruneau, C. H., Creusé, E., Gilliéron, P., & Mortazavi, I."Effect of the vortex dynamics on the drag coefficient of a square back Ahmed body": *European Journal of Mechanics-B/Fluids*, Vol 45, 1-11, 2014.

Daugherty, R. L. "Fluid mechanics with engineering applications". [S.l.]: Tata McGraw-Hill Education, 1989.

Dobrev, I.; Massouh, F. "Investigation of relationship between drag and lift coefficients for a generic car model". BULTRANS Proceedings, 2014.

Hucho, W. H. "Aerodynamics of road vehicles: from fluid mechanics to vehicle engineering". [S.l.]: Elsevier, 2013.

Hunt, J. C. R., Wray, A. A. and Moin, P. "Eddies, Streams, and Convergence Zones in Turbulent flows," Center for Turbulence Research Report CTR-S88, Stanford Univ., pp. 193–207, 1988.

Korkischko, I.; Meneghini, J. R. *Investigação experimental e simulação numérica do escoamento ao redor de um modelo automobilístico: corpo de Ahmed*. Trabalho de conclusão de curso em Engenharia Mecânica apresentado à Escola Politécnica da Universidade de São Paulo, 2006.

Menter, F. R. "Two-equation eddy-viscosity turbulence models for engineering applications". *AIAA journal*, v. 32, n. 8, p. 1598–1605, 1994.

Minguez, M., R. Pasquetti, and E. Serre. "High-order large-eddy simulation of flow over the "Ahmed body" car model." *Physics of fluids*, 20.9: 095101, 2008.

Möller, S.; Silvestrini, J. "Turbulência: fundamentos". Coleçao Cadernos de Turbulência. ABCM. Rio de Janeiro, v. 4, p. 1–32, 2004.

Ortega, J. M.; Salari, K. "Aerodynamic drag reduction apparatus for wheeled vehicles in ground effect". [S.l.]: Google Patents, US Patent 6,974,178, 2005.

Rafee, P. Moghimiand R. "Numerical and Experimental Investigations on Aerodynamic Behavior of the Ahmed Body Model with Different Diffuser Angles." *Journal of Applied Fluid Mechanics*, 11.4: 1101-1113, 2018.

Shadmani, S., et al. "Experimental investigation of flow control over an Ahmed body using DBD plasma actuator." *Journal of Applied Fluid Mechanics*, 11.5: 1267-1276, 2018.

Thacker, A. et al. “Effects of suppressing the 3d separation on the rear slant on the flow structures around an Ahmed body”. *Journal of Wind Engineering and Industrial Aerodynamics*, 2012, Elsevier, v. 107, p. 237–243.

Tunay, T.; Sahin, B.; Ozbolat, V. “Effects of rear slant angles on the flow characteristics of Ahmed body”. *Experimental Thermal and Fluid Science*, Elsevier, v. 57, p. 165–176, 2014.

Zhang, B. F., Y. Zhou, and S. To. "Unsteady flow structures around a high-drag Ahmed body." *Journal of Fluid Mechanics*, 777: 291-326, 2015.

7. RESPONSIBILITY NOTICE

The authors are the only responsible for the printed material included in this paper.